Single-Photon Detection by a Simple Silicon-on-Insulator Metal Oxide Semiconductor Field-Effect Transistor

doi: 10.1143/JJAP.51.06FE01

Single-Photon Detection by a Simple Silicon-on-Insulator Metal-Oxide-Semiconductor Field-Effect Transistor

Wei Du,* Hiroshi Inokawa, Hiroaki Satoh, and Atsushi Ono

Research Institute of Electronics, Shizuoka University, Hamamatsu 432-8011, Japan

We demonstrate that a simple silicon-on-insulator (SOI) metal-oxide-semiconductor field-effect transistor (MOSFET) which can be found in ordinary integrated circuits could operate as a single-photon detector at room temperature. A potential well created by $n^+p^-n^+$ junctions is used to trap photo-generated holes, which is detected as increased electron current in the bottom channel with a single-hole sensitivity. Although peaks in histograms of drain current are overlapped due to relatively small sensitivity to the holes, signal-to-noise ratio (SNR) is large enough to determine the position and height of each peak corresponding to the discrete number of trapped holes. In addition to this single-photon detection capability, the simple MOSFET structure could also benefit from the potentially high quantum efficiency (QE) since it includes fewer absorbing electrodes to the incident light.

* E-mail address: duwei@rie.shizuoka.ac.jp

1. Introduction

Single-photon detectors have found applications not only in life sciences[1,2] and cryptography[3,4] domain, but also in a wide variety of realm.[5-9] Since the demerits of conventional single-photon detectors, i.e. photomultiplier tubes (PMT) and avalanche photo diodes (APD), mainly stem from the carrier multiplication by high electric field, a carrier multiplication-free detector which directly detect photo-generated carriers one by one is expected to solve the problems.

Actually, single-photon detectors that used single-electron (or single-hole) tunneling transistor as a sensitive electrometer, and counted photo-generated carriers without multiplication, have been reported.[10-12] However, their operation temperatures were below 20 K, and could not readily replace PMT or APD. Recently, due to the miniaturization of silicon devices and the advancement in silicon-on-insulator (SOI) technology, we can obtain a metal-oxide-semiconductor field-effect transistor (MOSFET) with a single-electron sensitivity operating at room temperature.[13,14]

Some pioneering works[15,16] reported that short- and narrow-channel SOI MOSFET could operate as a single-photon detector, which realized the aforementioned operation mode and featured low dark counts and small operation voltage. Nevertheless, the counting rate of the detector was less than 10 s^{-1}. Recently, we presented a new type of single-photon detector based on a scaled-down (gate length L=65nm and channel width W=105nm) SOI MOSFET operating at room temperature,[17,18] which features improved quantum efficiency (QE), low dark counts and higher operation speed. However, in these devices, a special double-gate structure with a short lower gate (LG) and a long upper gate (UG) covering the entire p^--doped SOI area was used to create potential well below the LG to trap photo-generated holes. This complex structure resulted in still low QE, and might be an obstacle to general use.

In this report, a simple SOI MOSFET that can be found in ordinary integrated circuits is evaluated as a single-photon detector. A potential well created by $n^+p^-n^+$ junctions is used to trap photo-generated holes, and the presence of the holes is detected as increased electron current in the top or bottom channel.

2. Device Structure and Experimental Methods

Figure 1 shows cross-sectional view of (a) the previous and (b) present devices. In the former, negative V_{LG} together with V_{UG} bias creates potential well to trap photo-generated holes, while, in the latter, the $n^+p^-n^+$ doping structure creates the well. In both cases, positive V_{SUB} is applied to induce bottom electron channel that works as an electrometer to detect the presence of the trapped holes. In the present device (b), effective electrodes are 300-nm-long n^+ polycrystalline silicon (poly-Si) gate (LG) delineated above the 150-nm-wide, 50-nm-thick silicon layer with p^- dopant concentration less than 10^{15} cm^{-3}, n^+ source/drain region created in a self-aligned manner using the LG as a implantation mask,[19] and the substrate. The UG has no effect on the electrical characteristics and could be removed to enhance the QE, though the UG still remains in the present device [Fig. 1(b)] due to the experimental limitation i.e. reuse of the same photomasks for economic reasons.

For the detection of the trapped holes, both the top and bottom channels can be used, but the bottom one, enabled by applying $V_{LG}<0$ and $V_{SUB}>0$, is selected this time for the smaller current noise, which is sensitive to the bias condition.[20-28] In this case, photo-generated holes are trapped under the LG whereas back electron channel is used as an electrometer to detect the presence of the trapped holes. Photo-generation of carriers and their recombination will modulate the electron current, and can be observed as pulses.

3. Results and Discussion

Figure 2 shows the I_D-V_{LG} curves for different V_{SUB}'s from -10 to 10 V. As indicated in Fig. 2, the operation point is located where the curves are sparse and the electrons flow in the bottom channel. We should point out that both top and bottom channel can be used as an electrometer. However, it was necessary to select an appropriate biasing point to reduced the drain current noise. Generally, the low-frequency noise in MOSFETs is caused by the fluctuation of the charge state of the oxide traps close to the channel.[20] This fluctuation is reflected to the drain current noise, depending on the bias condition.[21-25] In case of SOI MOSFETs, the bias condition also affects the positions of noise-related traps, e.g. front channel, back channel, edge channel, etc.[26-28] Since the quality of oxides is not uniform and device dependent, in our particular device, we selected V_D, V_{LG}, and V_{SUB} of 0.05, −1, and 1 V, respectively, at which the noise level (i.e. the standard deviation of the drain current distribution) was minimized, and photo-generated pulse signal was clearly separated from the baseline current.

Figure 3 shows drain current waveforms for different incident light intensities at the wavelength of 550 nm at 300 K. We shift each waveform for clarity. It shows that, very similarly to our previous results,[18] pulse count is proportional to the photon incident rate. Moreover, different pulse levels can be seen clearly, indicating different number of holes trapped under the LG. The first, second, third and fourth levels correspond to the number of trapped holes of 0, 1, 2, and 3, respectively, although the step height is almost comparable to the noise amplitude. This is because the channel size of this device (L=300 nm and W=150 nm) is larger than that of the previous one, resulting in lower sensitivity, i.e., smaller current change per single trapped hole. As shown in Fig. 4, there is proportionality between the pulse generation rate and incident light intensity, suggesting that the obtained pulses correspond to single photons. The QE for the nominal active area of 300 × 150 nm^2 is 0.11% at 550 nm. Comparing with our previous

report,[18] active area in this device is entirely covered with the LG below the UG, while in previous device only small fraction is shielded. This small QE could be improved simply by removing the UG and/or replacing the LG with a transparent one.

The Coulomb interaction between holes is an important factor in the photon counting operation, because it may reduce the collection efficiency of the photo-generated holes and set the saturated number of trapped holes. According to the Fig. 4, as long as the count rate (i.e. hole generation rate) is less than 100 s^{-1}, the linearity is kept and the effect of the Coulomb interaction is not clearly observed. However, improvement in the maximum count rate, which is limited by the saturated number of trapped holes and the hole lifetime, remains to be tried in the future research.

Figures 5 (a)-5 (f) are histograms of drain currents corresponding to Fig. 3. The closed symbols are obtained data and solid lines are fitting curves with Gaussian distribution. The peaks from left to right in each graph correspond to the number of trapped holes of 0, 1, 2, and 3. When incident light intensity increases, more and more holes are generated, thus possibility of holes being trapped under LG increases, resulting in the higher peaks for more trapped holes. As we pointed out, unlike our previous results,[18] due to the relatively small sensitivity to the holes, the SNR is not large enough to completely separate each peak, resulting in overlapped peak distribution. Nevertheless, compared with the noise level (i.e., standard deviation), the peak-to-peak spacing is large enough to determine the position and height of each peak. Therefore, this device still has the ability to resolve the number of photons entering at the same time, if the QE could be sufficiently high.

Figure 6 shows probability of state f_i corresponding to the number of trapped holes i, as a function of generation rate R. The theoretical curves (solid lines) are obtained from rate

equations under steady condition, $f_i/\tau_i = f_{i-1}R$ and $\sum f_i = 1$, where τ_i is the hole lifetime of 83, 20 and 17 ms obtained as fitting parameters for the trapped holes of i=1, 2 and 3, respectively.

In the collective behavior of excess minority carriers, decay of the carrier density can be described with a single lifetime defined as $\Delta p/U$, where Δp is the excess carrier density and U is the net recombination rate per volume.[29,30] However, if we deal with the discrete number of holes, the lifetime is defined differently as an average dwell time τ_i before the transition takes place from the state of i holes to the state of $i-1$ holes. Such a lifetime is the inverse of the transition rate (i.e. the recombination rate), which naturally increase as i increases because the probability to encounter electrons for direct recombination or recombination centers for indirect recombination increases with i. Therefore, the hole lifetime τ_i depends on the number of trapped holes i.

In Fig. 6, experimental data (closed symbols) and theoretical ones coincide well, suggesting that this device has similar capability of single-photon detection as the previous one but with a simpler structure beneficial for wider usage.

4. Conclusion

In conclusion, a simple SOI MOSFET that can be found in ordinary integrated circuits can operate as a single-photon detector at room temperature. The potential well created by $n^+p^-n^+$ junctions is effective for photon response. Such detector also features small dark counts of less than 0.2 s^{-1} and small operation voltage of 1 V. The obtained QE of 0.11% at λ=550 nm is not so high, but could be raised simply by removing the UG since it does not play a role anymore in the proposed device. Based on these unique features together with its simple structure, the proposed single-photon detector may found varieties of applications in sensing and imaging.

Acknowledgments

The Authors are indebted to Keisaku Yamada of University of Tsukuba, Toyohiro Chikyo of National Institute of Materials and Science, Tetsuo Endoh of Tohoku University, Hideo Yoshino and Shigeru Fujisawa of Semiconductor Leading Edge Technologies, Inc. for their cooperation in the device fabrication.

REFERENCES

1) L. Alaverdian, S. Alaverdian, O. Bilenko, I. Bogdanov,E. Filippova, D.Gavrilov, B. Gorbovitski, M. Gouzman, G. Gudkov, S. Domratchev, O.Kosobokova, N. Lifshitz, S. Luryi, V. Ruskovoloshin, A.Stepoukhovitch, M. Tcherevishnick, G. Tyshko, and V. Gorfinkel: Electrophoresis **23** (2002) 2804.
2) B.L. Legendre, D.C. Williams, S. A. Soper, R. Erdmann, U. Ortmann, and J. Enderlein: Rev. Sci. Instrum. **67** (1996) 3984.
3) H. Kosaka, A. Tomita, Y. Nambu, T. Kimura, and K. Nakamura: Electron. Lett. **39** (2003) 1199.
4) A. Beveratos, R. Brouri, T. Gacoin, A. Villing, J. P. Poizat, and P. Grangier: Phys. Rev. Lett. **89** (2002) 187901.
5) W. Becker, A. Bergmann, M. A. Hink, K. König, K. Benndorf, and C. Biskup: Microsc. Res. Technol. **63** (2004) 58.
6) E. Moreau, I. Robert, J. M. Gérard, I. Abram, L. Manin, and V. Thierry-Mieg: Appl. Phys. Lett. **79** (2001) 2865.
7) G. N. Gol'tsman, O. Okunev, G. Chulkova, A. Lipatov, A. Semenov, K. Smirnov, B. Voronov, A. Dzardanov, C. Williams, and R. Sobolewski: Appl. Phys. Lett. **79** (2001) 705.
8) N. Gisin, G. Ribordy, W. Tittel, and H. Zbinden: Rev. Mod. Phys.**74** (2002) 145.
9) E. Knill, R. Laflamme, and G. J. Milburn: Nature **409** (2001) 46.
10) A. N. Cleland, D. Esteve, C. Urbina, and M. H. Devoret: Appl. Phys. Lett. **61** (1992) 2820.
11) O. Astafiev, S. Komiyama, T. Kutsuwa, V. Antonov, Y. Kawaguchi, and K. Hirakawa: Appl. Phys. Lett. **80** (2002) 4250.
12) R. Nuryadi, Y. Ishikawa, and M. Tabe: Phys. Rev. B **73** (2006) 045310.
13) K. Nishiguchi, A. Fujiwara, Y. Ono, H. Inokawa, and Y. Takahashi: Appl. Phys. Lett. **88** (2006) 183101.
14) K. Nishiguchi, C. Koechlin, Y. Ono, A. Fujiwara, H. Inokawa, and H. Yamaguchi: Jpn. J. Appl. Phys. **47** (2008) 8305.
15) A. Fujiwara, K. Yamazaki, and Y. Takahashi: Appl. Phys. Lett. **80** (2002) 4567.
16) K. Nishiguchi, Y. Ono, A. Fujiwara, H. Yamaguchi, H. Inokawa, and Y. Takahashi: Appl. Phys. Lett. **90** (2007) 223108.

17) H. Inokawa, W. Du, M. Kawai, H. Satoh, A. Ono and V. Singh: Adv. Mater. Res. **222** (2011) 3.
18) W. Du, H. Inokawa, H. Satoh, and A. Ono: Opt. Lett. **36** (2011) 2800.
19) L. C. Parrillo: in *VLSI Technology*, ed. S. M. Sze (McGraw-Hill, New York, 1983) Chap. 3.
20) Sh. Kogan: *Electronic Noise and Fluctuations in Solids* (Cambridge University Press, Cambridge, U.K., 1996) p. 234.
21) G. Ghibaudo: Solid-State Electron. **30** (1987) 1037.
22) G. Reimbold: IEEE Trans. Electron Devices **31** (1984) 1190.
23) C. Jakobson, I. Bloom, and Y. Nemirovsky: Solid-State Electron. **42** (1998) 1807.
24) E. Simoen and C. Claeys: Solid-State Electron. **43** (1999) 865.
25) Y. Nemirovsky, I. Brouk, and C. G. Jakobson: IEEE Trans. Electron Devices 48 (2001) 921.
26) S. Cristoloveanu and Sheng S. Li: *Electrical Characterization of Silicon-on-Insulator Materials and Devices* (Kluwer, Boston, MA, 1995) p. 297.
27) T. Elewa, B. Boukriss, H.S. Haddara, A. Chovet, and S. Cristoloveanu: IEEE Trans. Electron Devices **38** (1991) 323.
28) T. Elewa, B. Kleveland, S. Cristoloveanu, B. Boukriss, and A. Chovet: IEEE Trans. Electron Devices **39** (1992) 874.
29) S. M. Sze: *Physics of Semiconductor Devices* (Wiley, New York, 1981) 2nd ed., Chap. 1.
30) E. S. Yang: *Fundamentals of Semiconductor Devices* (McGraw-Hill, New York, 1978) Chap. 2.

Figure Captions

Fig. 1 (Color online) Cross-sectional view of (a) the previous[18] and (b) present devices. In the former, negative V_{LG} together with V_{UG} bias creates potential well to trap photo-generated holes, while, in the latter, the $n^+p^-n^+$ doping structure creates the well. In both cases, positive V_{SUB} is applied to induce bottom electron channel that works as an electrometer to detect the presence of the trapped holes. Note that, in the present device (b), the upper gate no longer play a role in creating the potential well, and could be removed without affecting the electrical characteristics, although the gate still remains due to the limitation in device fabrication. The thicknesses of buried oxide, SOI, LG oxide and insulator below the UG are 145, 50, 5, and 440 nm, respectively.

Fig.2 (Color online) I_D-V_{LG} curve with V_{SUB} as a parameter. Bottom electron channel is used as an electrometer and photo-generated holes are trapped below the LG.

Fig. 3 (Color online) Drain current waveforms at 300 K for different levels of light intensity at a wavelength of 550 nm. Each waveform is shifted for clarity. Base line current is about 1nA. V_D, V_{LG} and V_{SUB} are 0.05, -1, and 1V, respectively.

Fig. 4 (Color online) Pulse generation rate vs. incident light intensity. Slope of the fitting line is one.

Fig. 5 (Color online) Histograms of digitized drain currents corresponding to Fig. 3. 1st, 2nd, 3rd and 4th peaks correspond to the number of trapped holes of 0, 1, 2, and 3, respectively. Data acquisition time period and time step are 5 s and 488 μs, respectively, and 10,240 (=5 s/ 488 μs) data points (current values) are classified into bins with a width of 2 pA.

Fig. 6 (Color online) Probability of state obtained from Fig. 5 as a function of generation rate. States f_0, f_1, f_2 and f_3 correspond to the number of trapped holes of 0, 1, 2, and 3, respectively.

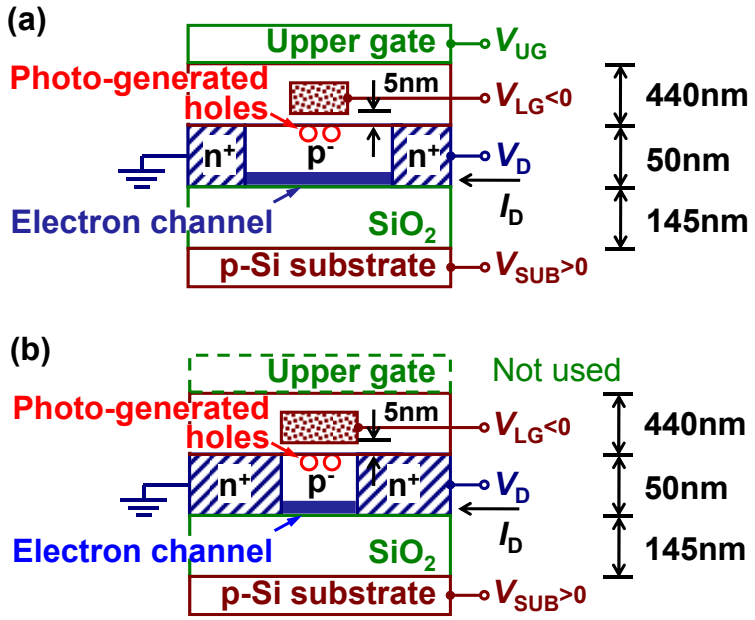

Fig. 1 (Color online) Cross-sectional view of (a) the previous[18] and (b) present devices. In the former, negative V_{LG} together with V_{UG} bias creates potential well to trap photo-generated holes, while, in the latter, the $n^+p^-n^+$ doping structure creates the well. In both cases, positive V_{SUB} is applied to induce bottom electron channel that works as an electrometer to detect the presence of the trapped holes. Note that, in the present device (b), the upper gate no longer play a role in creating the potential well, and could be removed without affecting the electrical characteristics, although the gate still remains due to the limitation in device fabrication. The thicknesses of buried oxide, SOI, LG oxide and insulator below the UG are 145, 50, 5, and 440 nm, respectively.

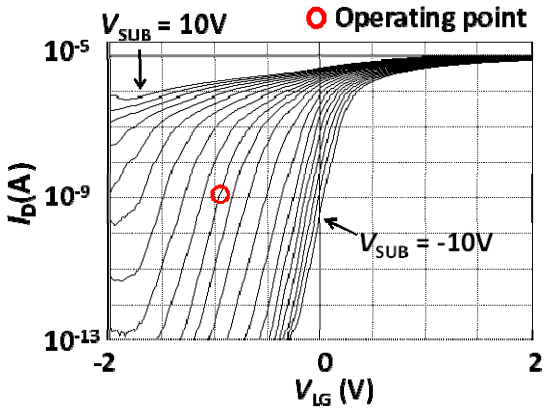

Fig.2 (Color online) I_D-V_{LG} curve with V_{SUB} as a parameter. Bottom electron channel is used as an electrometer and photo-generated holes are trapped below the LG.

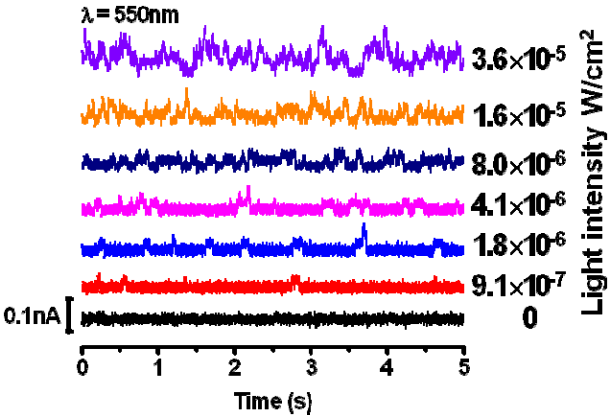

Fig. 3 (Color online) Drain current waveforms at 300 K for different levels of light intensity at a wavelength of 550 nm. Each waveform is shifted for clarity. Base line current is about 1nA. V_D, V_{LG} and V_{SUB} are 0.05, -1, and 1V, respectively.

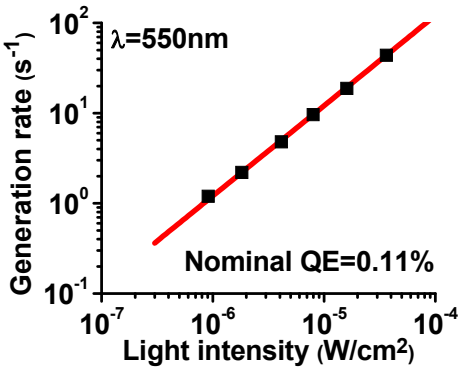

Fig. 4 (Color online) Pulse generation rate vs. incident light intensity. Slope of the fitting line is one.

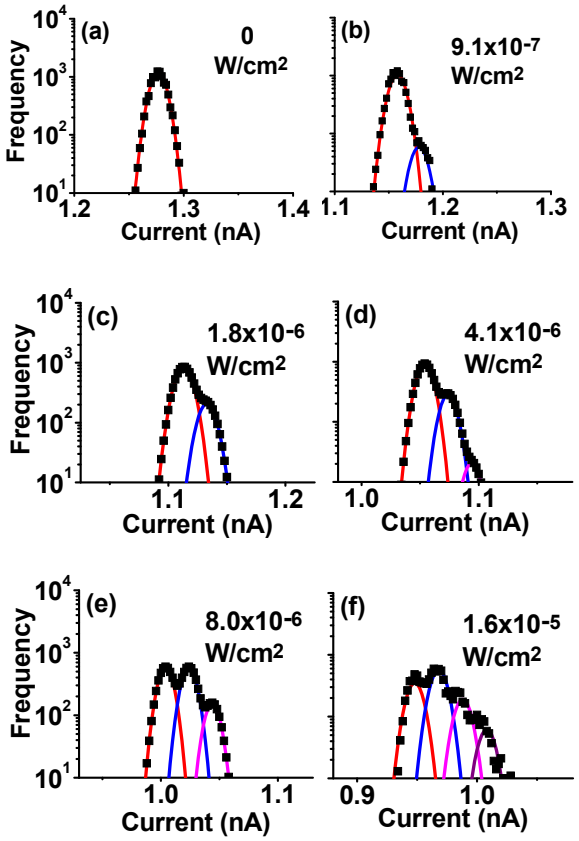

Fig. 5 (Color online) Histograms of digitized drain currents corresponding to Fig. 3. 1st, 2nd, 3rd and 4th peaks correspond to the number of trapped holes of 0, 1, 2, and 3, respectively. Data acquisition time period and time step are 5 s and 488 μs, respectively, and 10,240 (=5 s/ 488 μs) data points (current values) are classified into bins with a width of 2 pA.

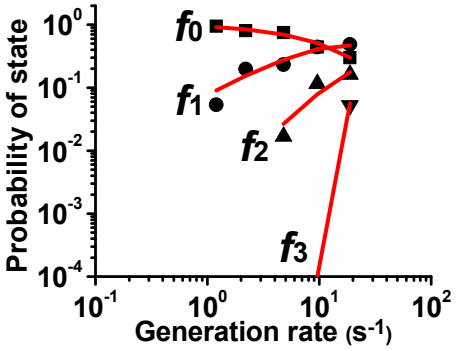

Fig. 6 (Color online) Probability of state obtained from Fig. 5 as a function of generation rate. States f_0, f_1, f_2 and f_3 correspond to the number of trapped holes of 0, 1, 2, and 3, respectively.